Journal of Power Sources 201 (2012) 151–158

Contents lists available at SciVerse ScienceDirect

Journal of Power Sources

journal homepage: www.elsevier.com/locate/jpowsour

Fuel cell performances at optimized Nafion and $Ru_{85}Se_{15}$ loadings in cathode catalyst layer

Qiaoming Zheng[a], Xuan Cheng[a,b,*], Ting-Chu Jao[c,d], Fang-Bor Weng[c,d,**], Ay Su[c,d], Yu-Chun Chiang[c,d]

[a] Department of Materials Science and Engineering, Xiamen University, Xiamen Fujian 361005, China
[b] Fujian Key Laboratory of Advanced Materials, Xiamen University, Xiamen Fujian 361005, China
[c] Department of Mechanical Engineering, Yuan Ze University, Zhongli Taoyuan 320, Taiwan
[d] Fuel Cell Center, Yuan Ze University, Zhongli Taoyuan 320, Taiwan

ARTICLE INFO

Article history:
Received 21 September 2011
Received in revised form 2 November 2011
Accepted 3 November 2011
Available online 10 November 2011

Keywords:
PEM fuel cells
Selenium modified ruthenium
Nafion content
Ru load
Electrochemical impedance spectroscopy

ABSTRACT

The citric acid treated carbon supported $Ru_{85}Se_{15}$ catalysts are synthesized by microwave assisted polyol method at the optimal solution pH = 7. The catalyst coated membrane method with ultrasonic-spray technique is employed to prepare electrodes without hot press step. The cell performances with different Nafion contents and Ru loads in the cathode catalyst layer are systematically examined in both H_2/air and H_2/O_2 fuel cells at 65 °C under ambient pressure. The surface morphologies of membrane electrode assemblies and the interfacial characteristics of single cells are studied using scanning electron microscopy and electrochemical impedance spectroscopy, respectively. The Nafion content is optimized to be 33% when the catalyst loadings are lower than 0.8 and 0.6 mg Ru cm^{-2} in the H_2/air and H_2/O_2 fuel cells, respectively, but reduced to 20% at the higher Ru loads. The maximum peak power densities of 190 mW cm^{-2} at 620 mA cm^{-2} and 400 mW cm^{-2} at 1430 mA cm^{-2} are achieved in the H_2/air and H_2/O_2 fuel cells, respectively, with 0.27 mg Ru cm^{-2} and 33% Nafion. The best catalyst utilizations are obtained at 0.14 mg Ru cm^{-2} with 33% Nafion, resulting in the maximum peak power densities per unit mass Ru of 917 and 2460 mW mg^{-1} in the H_2/air and H_2/O_2 fuel cells, respectively.

1. Introduction

Selenium modified ruthenium (Ru_xSe_y) catalysts have been receiving more and more attention as potential alternatives to platinum-based cathode catalysts in polymer electrolyte membrane (PEM) fuel cells because of their comparable catalytic activity toward oxygen reduction reaction (ORR), low cost, high abundance and, in particular, a high tolerance to small organic molecules [1]. Lower catalyst loading with an optimum Nafion content in the catalyst layer is necessary for maximizing cell performance. The catalyst coated gas diffusion medium (GDM) method has been developed to utilize carbon supported platinum (Pt/C) to incorporate Nafion ionomer within the catalyst layers [2]. It was found that the gas diffusion electrodes (GDEs) fabricated by the ultrasonic-spray method with 0.05 mg Pt cm^{-2} exhibited a peak power rating of 10.9 W mg^{-1} compared to 9.8 W mg^{-1} with the same loading for the hand-painted GDEs [3]. However, the GDM method caused the structural deformation during the hot press step and the catalyst loss through the porous gas diffusion layer (GDL). As an alternative to the GDM, the catalyst coated membrane (CCM) method has been employed without the hot press step. The interfacial characteristics between the electrolytes and the catalyst layers were enhanced because the catalyst layers are directly coated onto the membranes [4,5].

The Nafion ionomer is generally impregnated into the surface of catalyst layers to increase the three dimensional reaction zones where only these catalysts are electrochemically active. The Nafion ionomer also acts as a proton conductor, binding materials to impart mechanical stability and hydrophilic agents to retain moisture and prevent membrane from dehydration [2]. The effects of Nafion ionomer content and Pt/C catalyst load on the cell performance have been previously studied [6–12]. The optimum Nafion content should depend on the Pt loading since it affected the triple phase boundary [6]. The electrode where the Nafion ionomer was impregnated on the surface of catalyst layer showed better cell performance than that of in the inside of catalyst layer [7]. The optimal Nafion content was further determined to be 56% with 0.4 mg cm^{-2} of Pt/C load [7].

Compared with Pt or Pt-based catalysts, the effects of Nafion content and catalyst load on cell performance using $Ru_{85}Se_{15}$

* Corresponding author at: Department of Materials Science and Engineering, Xiamen University, Xiamen Fujian 361005, China. Tel.: +86 592 218 5599; fax: +86 592 218 3937.
** Corresponding author at: Department of Mechanical Engineering, Yuan Ze University, Zhongli Taoyuan 320, Taiwan. Tel.: +886 3 4618691; fax: +886 3 4555574.
E-mail addresses: xcheng@xmu.edu.cn (X. Cheng), fangbor@saturn.yzu.edu.tw (F.-B. Weng).

0378-7753/$ – see front matter.
doi:10.1016/j.jpowsour.2011.11.011

as a cathode catalyst have not been previously studied. Accordingly, no optimized Nation contents have been determined. The maximum power density of 141 mW cm^{-2} at 450 mA cm^{-2} was reported with the optimized 0.4 mg Ru cm^{-2} of Ru_xSe_y and 65% Nafion at 80 °C under 30/40 psi back pressure in a H_2/O_2 single cell test [13], while 38 mW cm^{-2} at 200 mA cm^{-2} in the optimized 1.9 mg Ru(44%)Se(2.8%)/XC72 cathode catalyst layers with 30% Nafion at 80 °C under ambient pressure for a direct methanol fuel cell [14]. Recently, under non-optimized conditions the promising peak power densities as high as 126 mW cm^{-2} at 510 mA cm^{-2} and 336 mW cm^{-2} at 1230 mA cm^{-2} in the H_2/air and H_2/O_2 single cell tests, respectively, were obtained with 0.14 mg Ru cm^{-2} of $Ru_{85}Se_{15}$ supported on citric acid treated XC-72R and 33% Nafion in our previous work [15].

This work was carried out to systematically investigate the effects of Nafion ionomer content and $Ru_{85}Se_{15}$ catalyst load within the electrode on the single cell performance. The $Ru_{85}Se_{15}$ catalysts were synthesized by microwave assisted polyol synthesis method. The electrodes with different Ru loads and Nafion contents in the cathode catalyst layer were prepared by the ultrasonic-spray technique and were examined in both H_2/air and H_2/O_2 PEM fuel cells. The interfacial characteristics were studied by electrochemical impedance spectroscopy and the interfacial parameters were evaluated by fitting with the equivalent circuit. The best cell performance and best catalyst utilization were determined with the optimized Nation contents and Ru loads.

2. Experimental

2.1. Preparation of catalysts

The $Ru_{85}Se_{15}$ catalysts were prepared with citric acid (CA) treated commercial carbon blacks Vulcan XC-72R (Cabot Corp., BET: 237 m^2 g^{-1}) using microwave assisted polyol synthesis method at the optimized initial solution pH = 7 as determined previously [15]. The weight ratios of $Ru_{85}Se_{15}$ and Ru in the $Ru_{85}Se_{15}$/CA-XC72R catalyst were approximately 25% and 22%, respectively.

2.2. Preparation of membrane electrode assemblies (MEAs)

The 40% Pt/C (Johnson Matthey) was placed in a beaker and wetted with a few drops of water. The 5% Nafion solutions (DuPont) and ethanol were added and ultrasonicated for 30 min. The Nafion content was in term of wt% of Nafion (dry weight of Nafion ionomer divided by the total weights of catalyst and Nafion ionomer, multiplied by 100). The Pt/C ink with 33% Nafion was prepared as the anode catalyst ink. Meanwhile the 25% $Ru_{85}Se_{15}$/CA-XC72R and 5% Nafion solutions were well distributed in ethanol and used as the cathode catalyst ink.

The membrane electrode assemblies (MEAs) were fabricated using the Sono-Tek 'Exacta-coat' ultrasonic-spray instrument operating at 48 kHz which includes an ultrasonic syringe and an ultrasonic-spray head to obtain the uniform and smooth catalyst layer. The spray head was controlled to create a specific pattern for different repetitions to spray on Nafion-212 membranes (Dupont). The MEAs were prepared with 0.256 mg Pt cm^{-2} for anode and different catalyst loads (0.14, 0.27, 0.48, 0.61, 1.02 mg Ru cm^{-2}) with various Nafion contents (20, 33, 38, 43, 50%) in the cathode catalyst layer.

2.3. Single cell tests

The catalyst coated membranes were placed between two silicone gaskets, sandwiched by two GDLs (SGL carbon AG, Germany), then assembled into 5 cm^2 single cells. The polarization curves were measured using a fuel cell test station (850C, Scribner Associates Inc.). The single cell tests were operated at 65 °C under ambient pressure. The flow rates of H_2 were 100 and 250 ml min^{-1}, respectively, in the H_2/air and H_2/O_2 single cell tests with the flow rates of air and O_2 being 250 ml min^{-1}. After the polarization measurements, the single cell was stabilized at 0.4 V for 10 min and the impedance measurements were made at 0.4 V with a frequency range of 10 kHz–0.1 Hz. The data were curve-fitted with ZSimpWin software (Princeton Applied Research) utilizing complex non-linear least square errors technique. The tested MEAs were removed from the single cell. The MEAs before and after each single cell test were cut by a blade in liquid nitrogen to obtain the surface and cross-sectional morphologies using LEO1530 field emission scanning electron microscope (Oxford Instrument, Germany). The surface elemental compositions of cathode catalyst layers were also characterized by the build-in energy dispersive X-ray spectrometer.

3. Results and discussion

3.1. Effect of Nafion contents on cell performance

The polarization and power density curves obtained with different Nafion contents and Ru loads in the H_2/air single cell tests at 65 °C under ambient pressure are shown in Fig. 1. At low catalyst loading of 0.14 mg Ru cm^{-2} as depicted in Fig. 1(a), the cell performance was slightly improved when the Nafion contents went up from 20% to 33% where the maximum peak power density (P_{max}) of 127 mW cm^{-2} was reached at 506 mA cm^{-2}. Further increases to 50% resulted in a significant decayed cell performance. The apparent enhanced cell performances were observed with 0.27 mg Ru cm^{-2} as evident in Fig. 1(b). The best P_{max} of 190 mW cm^{-2} was obtained at 620 mA cm^{-2} with 33% Nafion, which is 50% higher than that obtained at 0.14 mg Ru cm^{-2}. The cell performances also became worse with the Nafion contents larger than 33%. At very high catalyst loading of 1.02 mg Ru cm^{-2} as seen in Fig. 1(c), the best performance was achieved at 20% Nafion. The cell performance degraded all the way with the increases of Nafion content.

The polarization and power density curves were measured in the H_2/O_2 fuel cells under the same conditions as those used in Fig. 1 except replacing air by oxygen. The results are presented in Fig. 2. Compared with Fig. 1, the cell performances were remarkably enhanced with oxygen, and the similar effects of Nafion contents and Ru loads were observed. The best P_{max} values were found to be 339 and 400 mW cm^{-2} with 33% Nafion at 0.14 and 0.27 mg Ru cm^{-2}, respectively, while 325 mW cm^{-2} with 20% Nafion at 1.04 mg Ru cm^{-2} in the H_2/O_2 single cells.

In an effort to understand possible changes occurred within the MEAs by variations of Nafion contents and Ru loads, the surface and cross-sectional morphologies, as well as the elemental information of cathode catalyst layers from the fresh and tested MEAs under different Nafion contents and Ru loads were obtained. Fig. 3(a) shows a typical electrode including micro-porous layer (MPL), GDL and MEA consisting of membrane, anode catalyst and cathode catalyst layers (bottom left image in Fig. 3(a)). The cross-sectional micrographs of fresh MEAs revealing the apparent thicknesses of cathode catalyst layers at 33% Nafion with low loading of 0.14 mg Ru cm^{-2} (Fig. 3(b)) and high loading of 0.61 mg Ru cm^{-2} (Fig. 3(d)), as well as at 50% Nafion with 0.14 mg Ru cm^{-2} (Fig. 3(f)) are also provided. The surface morphologies of $Ru_{85}Se_{15}$ catalysts and the corresponding EDX spectra are illustrated in Fig. 3(c, e and g). A lot of gas pores were observed from the cross-sectional morphology (bottom right image in Fig. 3(a)) and the surface morphologies of cathode catalyst layers (Fig. 3(c, e and g)). The $Ru_{85}Se_{15}$ catalysts distributed uniformly and attached to the carbon supports well. The thickness

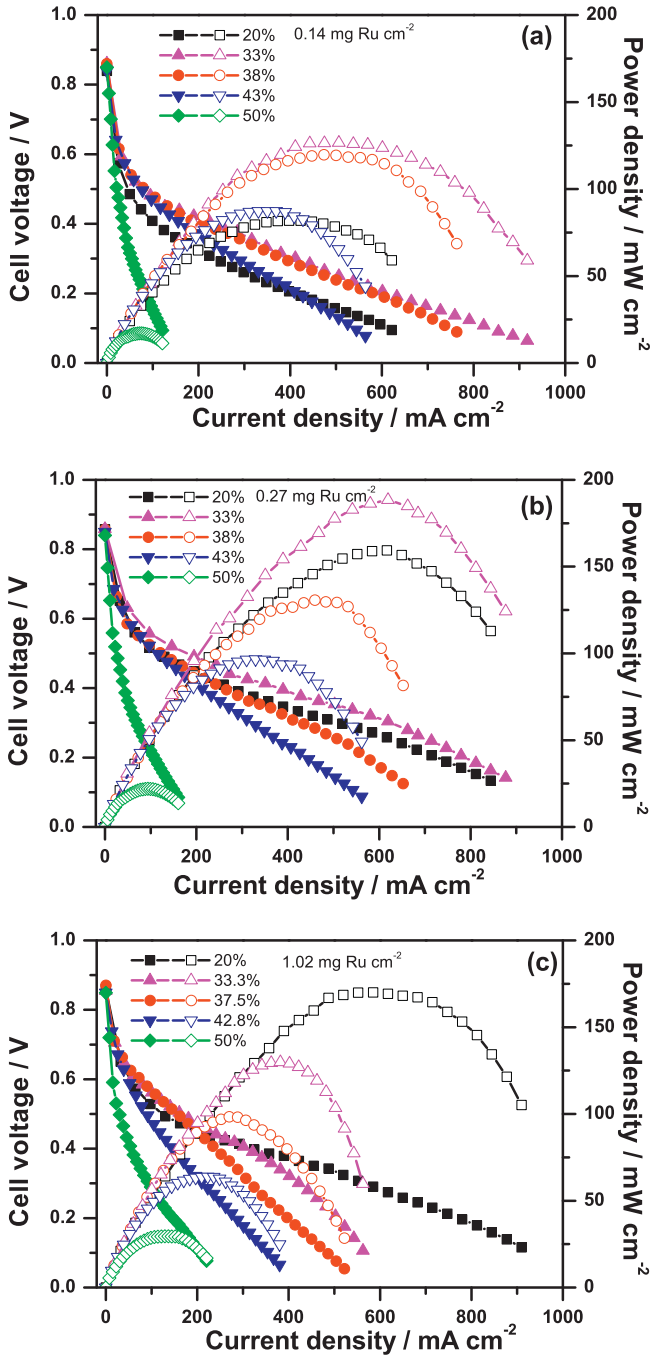

Fig. 1. Polarization and power density curves obtained with different Nafion contents and catalyst loads in the H_2/air single cell tests at 65 °C under ambient pressure. H_2/air: 100/250 ml min^{-1}, anode: 40% Pt/C, 0.256 mg Pt cm^{-2}, cathode: $Ru_{85}Se_{15}$/CA-XC72R, Nafion-212.

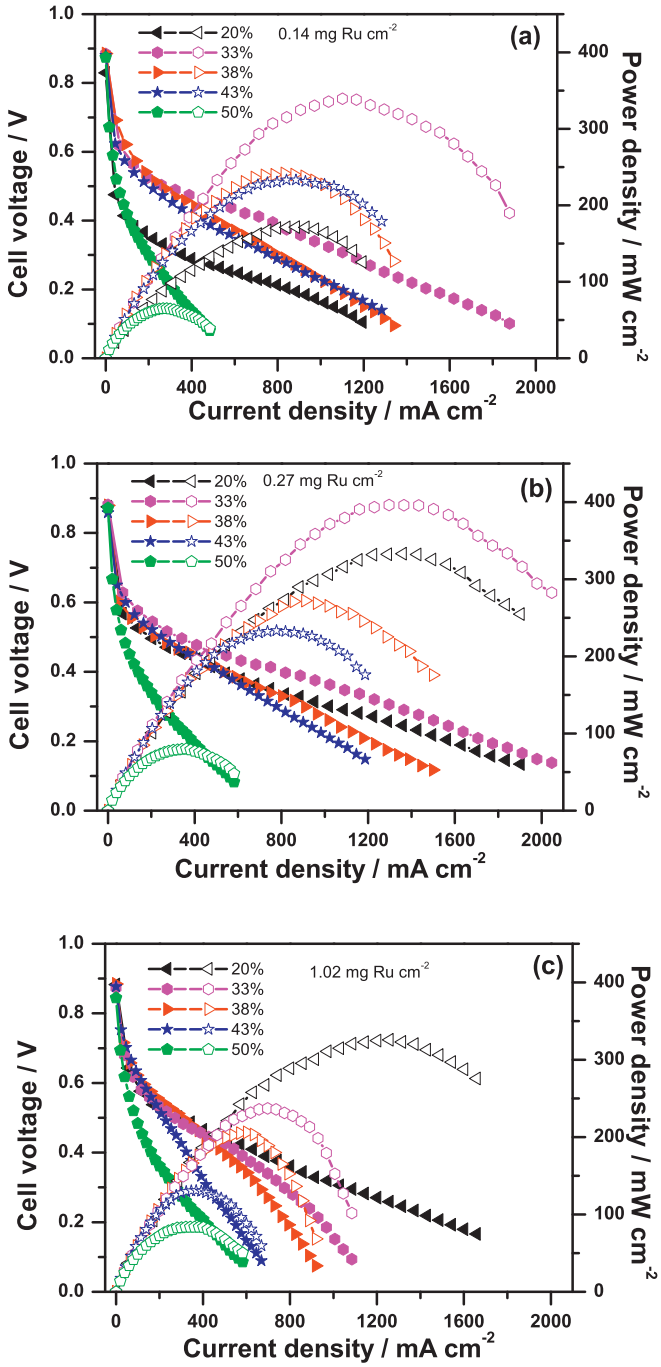

Fig. 2. Polarization and power density curves obtained with different Nafion contents under different catalyst loads in the single cell tests at 65 °C and ambient pressure. H_2/O_2: 250/250 ml min^{-1}, anode: 40% Pt/C, 0.256 mg Pt cm^{-2}, cathode: $Ru_{85}Se_{15}$/CA-XC72R, Nafion-212.

of catalyst layers would be directly affected by the amounts of catalyst and Nafion content. With the nearly same thicknesses of anode catalyst layers and membranes, the thickness of cathode catalyst layer increased approximately from 11 to 28 μm with the Ru loads going up from 0.14 to 0.61 mg cm^{-2} (Fig. 3(b and d)), while 11 to 15 μm with the Nafion contents increasing from 33 to 50% (Fig. 3(b and f)). In the cathode catalyst layer the ORR occurs at the triple phase boundary involving oxygen, electrolyte and catalyst [16]. The cell performance is mainly determined by the amount of the triple phase boundary. Oxygen diffuses through three different components: gas pores, liquid water and electrolyte. It was reported that for Pt/C oxygen diffusion in gas pores was the dominant process and diffusion in the other two components might be neglected when the volume of gas pores was sufficiently high [8]. In the present case the oxygen diffusion in gas pores has been mainly considered. The quantity of catalyst sites and the thickness of catalyst layers would be directly affected by the amounts of catalyst. The use of higher catalyst loading increases not only the active catalyst sites, which is beneficial to cell performance, but also increases the thickness of cathode catalyst layer, which may lead to poor cell performance due to the mass transport limitations including oxygen diffusion, proton transfer and water drainage. Unfortunately, there was no suitable method available to quantitatively determine the active

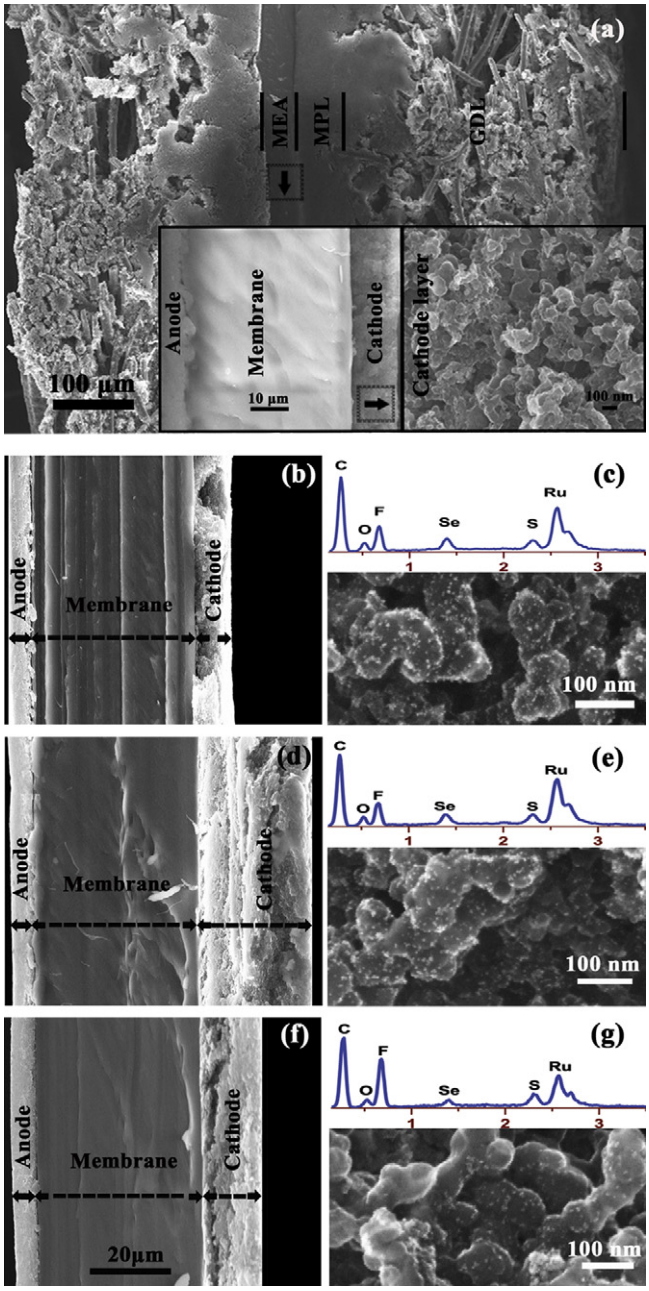

Fig. 3. SEM images: (a) cross-section of the anode and cathode electrodes. The insets are MEA (left) and cathode catalyst layer (right) with 0.27 mg Ru cm^{-2} and 33% Nafion; (b, d and f) cross-sections of fresh MEAs and (c, e, and g) surfaces of cathode catalyst layers with (b and c) 0.14 mg Ru cm^{-2} and 33% Nafion, (d and e) 0.61 mg Ru cm^{-2} and 33% Nafion, (f and g) 0.14 mg Ru cm^{-2} and 50% Nafion. The corresponding EDX spectra are also included.

surface of Ru_xSe_y catalysts in MEAs since Ru_xSe_y did not absorb methanol or CO [14]. Compared with 23% F and 18% Ru in Fig. 3(c), as well as 22% F and 20% Ru in Fig. 3(e), the weight proportions of F and Ru elements in Fig. 3(g) were 34% and 12%, respectively. Fewer catalysts observed in Fig. 3(g) might be due to the abundant Nafion contents (50%). The Nafion ionomer binds the catalysts to impart mechanical stability, acts as no only a proton conductor to expand the electrochemically active region into the bulk catalyst layer, but also hydrophilic agents to retain moisture and prevent membrane from dehydration. The addition of appropriate amount of Nafion electrolyte should enlarge the triple phase boundary and simultaneously heighten the degree of catalyst utilization. Too less Nafion

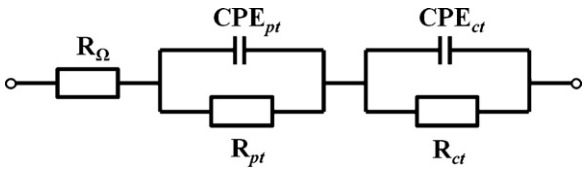

Fig. 4. The equivalent circuit used to fit the impedance data.

contents may result in poor contact of electrolyte with catalyst since proton conducting Nafion ionomer fragments may become discontinuous [6], and too much Nafion may block catalyst surface atoms and prevent them from adsorbing and activating oxygen. The high Nafion content may also result in water flooding which blocks the catalyst sites and arouses mass transport polarization. Therefore, the optimum Nafion and catalyst loads require a good balance among oxygen transport, catalyst sites and proton migration within the catalyst layer.

3.2. Effect of Nafion contents on cell interfacial characteristics

The equivalent circuit selected for the representation of the catalyst/Nafion interface is illustrated in Fig. 4, where R_Ω, R_{pt} and R_{ct} are the ohmic resistance, proton transfer resistance and charge transfer resistance, respectively. The constant phase element (CPE) replaces the conventional double-layer capacitance because the capacitance caused by the double-layer charging is distributed along the length of the pores in the porous electrode [17,18]. The form of CPE with impedance can be written as

$$Z_{CPE} = \frac{1}{Y_O(j\omega)^n} \quad (1)$$

where $j = \sqrt{-1}$, ω is the angular frequency and Y_O is a constant with dimension of $F\,s^{n-1}$. The case $n = 1$ in Eq. (1) recovers a perfect capacitor. The goal of an equivalent circuit is to split up the total impedance of a fuel cell into single impedance elements, which represent the individual parts of a fuel cell.

The impedance data corresponding to the cell performances in Fig. 1 were collected and are fitted using the equivalent circuit given in Fig. 4. The results are presented as Nyquist and Bode plots in Fig. 5. Experimentally the pure hydrogen could minimize the anode effect, and the high airflow of 250 ml min^{-1} used in this study would lessen the mass transport effect through the GDL. Therefore, the single semicircles are seen in Fig. 5(a–c) when the electrode process is dominated by the ORR interfacial kinetics only, and can be used to study the cathode kinetic behavior of the fuel cell directly without other complications. The high frequency intercept of a single impedance arc on the real axis, R_Ω, represents the total ohmic resistance of the cell, which includes all the contact resistances between components and ohmic resistance of the cell components such as the membrane, catalyst layers, GDLs, and bipolar plates. The nearly linear responses at the high frequency region in Nyquist plots (the insets in Fig. 5(a–c)) were observed because of the proton conductivity limitation within the catalyst layer. This straight line, which is typical of a porous electrode, can provide information about the localization and distribution of the catalyst and electrolyte in the layer. The effect of proton transfer was not negligible from the observation of the insets in Fig. 5(a–c). This impedance response corresponds to the equivalent circuit composed of CPE_{pt} and R_{pt}. The diameter of the kinetic loop, R_{ct}, is a measure of the charge transfer resistance of ORR [19,20]. The charge transfer arc shrank with the increase of electrochemical kinetics which is associated with an extension of the three-phase interface. This is consistent with the corresponding cell performance obtained as provided in Fig. 1. However, the mass transport losses in this study cannot be represented by introducing the conventional Warburg element,

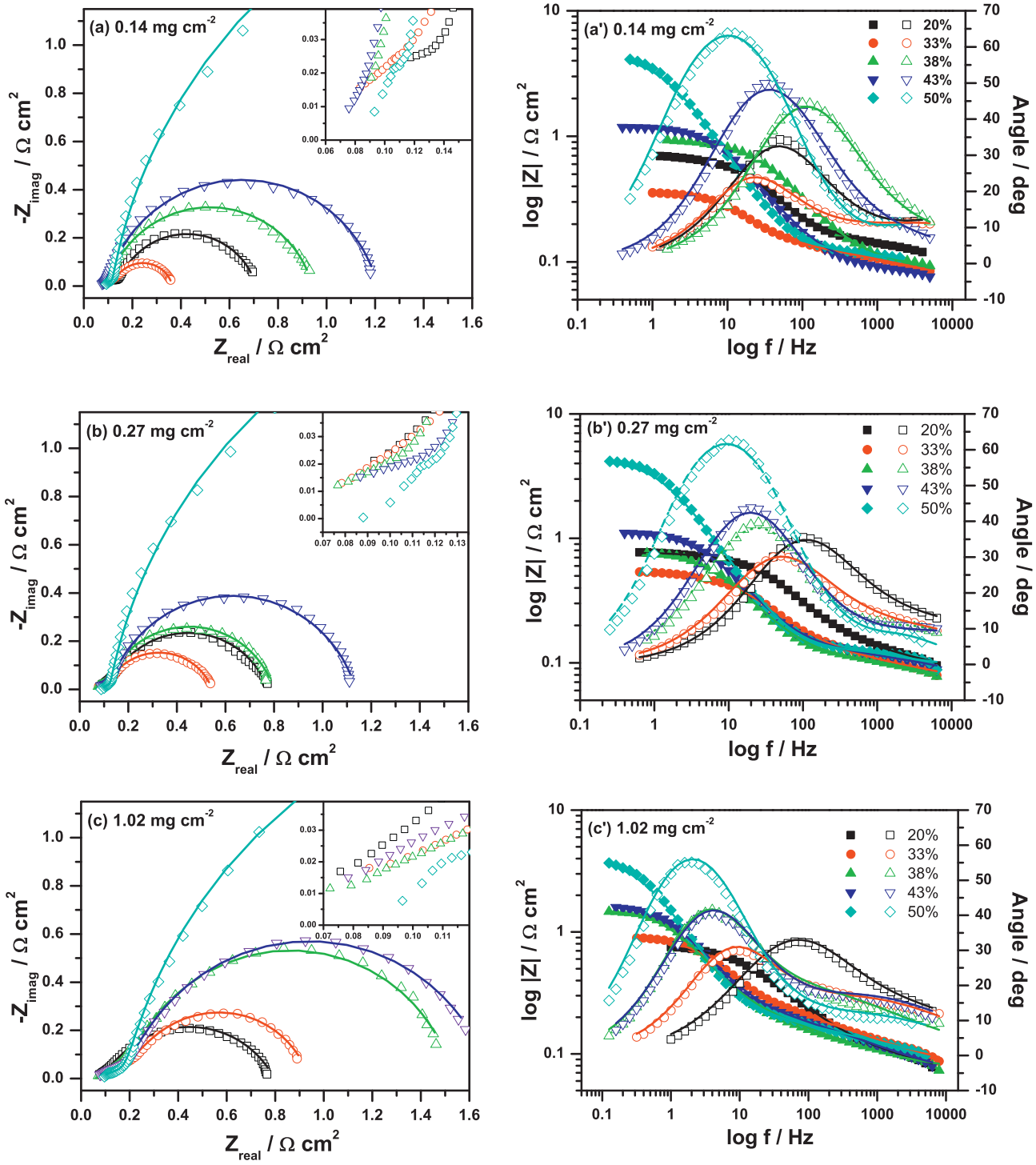

Fig. 5. Nyquist plots (a–c), Bode magnitude and phase angle plots (a′–c′) obtained with various Nafion contents (□20% ○33% △38% ▽43% ◊50%) under different catalyst loads in the H_2/air single cell tests at 0.4 V from 0.1 Hz to 10 kHz.

which is expected as an additional semicircle or a straight line in the Nyquist plot at low frequencies. A parallel circuit containing a CPE_{ct} and R_{ct} was used to analyze the ORR kinetics which is also determined by oxygen transport.

The transport limitation results from an increase in a pathway through which the gas has to permeate, diffuse, or migrate. The diffusion process is related to an oxygen concentration gradient in the Pt/C cathode including the GDL and gas channel which become quite small using the high flow air or pure oxygen [21,22]. The diffusion process is predominated at low frequency region, for example, at frequencies smaller than 1 Hz for Pt/C, while the charge transfer process corresponds to intermediate and high frequencies. As can be seen from the corresponding Bode plots in Fig. 5(a′–c′), the shifts in frequencies to 10 Hz (related to the diffusion process) at both 0.14 and 0.27 mg Ru cm^{-2} as compared with 1 Hz at 1.02 mg Ru cm^{-2} might be caused by the differences in the thicknesses of catalyst layer which are much thinner at low Ru loads. The triple phase boundary was also determined by the catalyst sites, and the addition of Nafion from 20% to 33% would increase the catalyst utilization. Thus, the cell impedances became

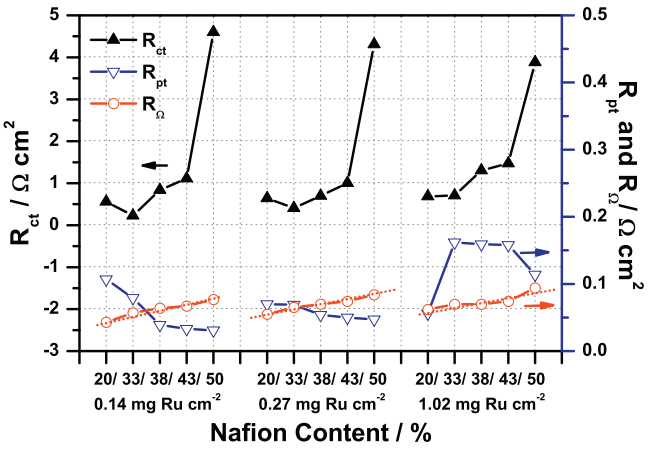

Fig. 6. Variations of interfacial resistances with the Nafion contents and catalyst loads.

smaller and the peak phase angles shifted toward lower frequencies (Fig. 5(a′ and b′)) similar to Pt/C [18]. At larger Ru loads, the catalyst layer became thicker and the gas pores became smaller with increasing the Nafion concentrations. The proton conductivity would be enhanced with larger Nafion loads. However, too small pores inside too thick catalyst layer may introduce severe mass transport limitations by retarding the gas access to active sites. Thereby, at the very high catalyst loading such as 1.02 mg Ru cm^{-2}, decreasing Nafion ratio led to the reduction in mass transport limitation through which the oxygen diffuses to the catalyst sites. The smallest impedance and phase angle shifting to lower frequency were observed with 20% Nafion which led to the best performance.

To more quantitatively analyze the changes of cathode catalyst layers by variations of Nafion contents and Ru loads, three interfacial resistances, namely R_Ω, R_{pt} and R_{ct}, are plotted against the Nafion contents and Ru loads in Fig. 6. It is obvious that the R_Ω (opened circles) increased almost linearly with the increase of Nafion contents in the range of 43–96 mΩ cm^2, implying that the catalyst layer became thicker. The magnitude of R_{ct} was 1 or 2 orders larger than R_{pt}. At both 0.14 and 0.27 mg Ru cm^{-2}, the R_{ct} reduced first at 33% and then went up, while the R_{pt} dropped with the increases of Nafion contents, indicating that the ORR taking place at the triple phase boundary became more difficult at higher Nafion concentrations, although the proton transfer became faster. At 1.02 mg Ru cm^{-2} the R_{ct} climbed all the way with the increase of Nafion contents owing to the thicker catalyst layers by using very high Ru load. The R_{pt} increased appreciably at 33% and remained virtually unchanged with the increase of Nafion contents from 33% to 43% since the proton transfer required a longer path due to the oxygen diffusion limitations. For the thicker catalyst layer the beneficial proton transfer (positive) and detrimental oxygen diffusion (negative) by the addition of 23–33% Nafion were not completely compensated, this led to severe degradation in the cell performance as evident in Fig. 1(c). At 50% Nafion a rapid rise in R_{ct} was observed at the three levels of Ru loads, which might be caused by the partially Nafion-coated active sites on the catalyst surfaces and very thick catalyst layers. Although the proton transport became fast (smaller R_{pt}), the more heavily retarded or impeded oxygen diffusion (very large R_{ct}) was responsible for the very poor cell performances obtained with 50% Nafion at the three levels of Ru loads (Fig. 1). It is, therefore, not always good to increase the Nafion content on a cathode, and an optimal amount of the Nafion ionomer to facilitate both the proton conduction and oxygen diffusion to the catalyst sites is necessary.

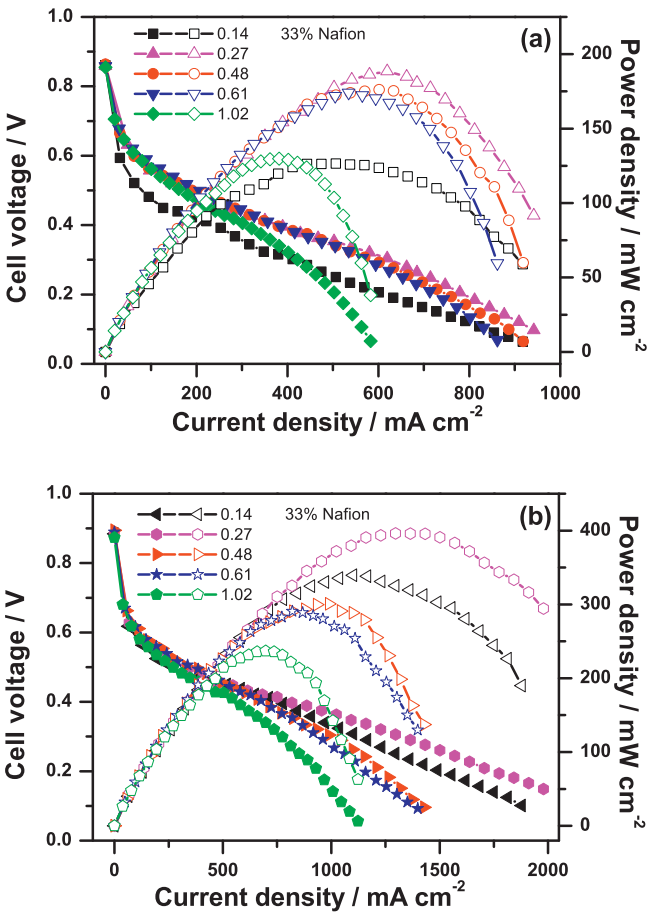

Fig. 7. Polarization and power density curves obtained at the optimized Nafion content of 33% under different catalyst loads in the single cell tests at 65 °C under ambient pressure with (a) H_2/air: 100/250 ml min^{-1} and (b) H_2/O_2: 250/250 ml min^{-1}. Anode: 40% Pt/C, 0.256 mg Pt cm^{-2}, cathode: $Ru_{85}Se_{15}$/CA-XC72R, Nafion-212.

3.3. *Effect of Ru loads on cell performance*

At the optimal 33% Nafion in the cathode catalyst layers based in Figs. 1 and 2, the polarization and power density curves were obtained with different Ru loads in the H_2/air and H_2/O_2 fuel cells, and the results are compared in Fig. 7. It is interesting to note that in Fig. 7(a) the cell performances were almost the same at the low current density region for the catalyst loads of 0.27, 0.48 and 0.61 mg Ru cm^{-2} in the H_2/air fuel cells, while appreciably different from each other at the current densities higher than 550 mA cm^{-2}. The highest P_{max} was obtained with 0.27 mg Ru cm^{-2} due to the good trade of between the numbers of catalyst sites (more than 0.14 mg Ru cm^{-2}) and the thickness of catalyst layers (thinner than 0.48 and 0.61 mg Ru cm^{-2}). When the catalyst layer was comparatively thinner (less than 0.27 mg Ru cm^{-2}), the active sites may become the main rate-determining step, while at high loadings and high Nafion contents, the catalyst layer may become thicker and oxygen diffusion becomes the main rate-determining step. Too less or too much Ru loads resulted in poor cell performance. In the H_2/O_2 fuel cells as seen in Fig. 7(b), the cell performance significantly improved with oxygen. The best cell performance was also achieved at 0.27 mg Ru cm^{-2}. The major differences in the H_2/air and H_2/O_2 fuel cells are the charge transfer step, which is becoming dominant as increasing the Ru loads by decreasing the oxygen diffusion limitation. The highest P_{max} values obtained at 0.27 mg Ru cm^{-2} were 190 mW cm^{-2} at 620 mA cm^{-2} and 400 mW cm^{-2} at 1430 mA cm^{-2}, corresponding to P_{max}^{mass} (P_{max}

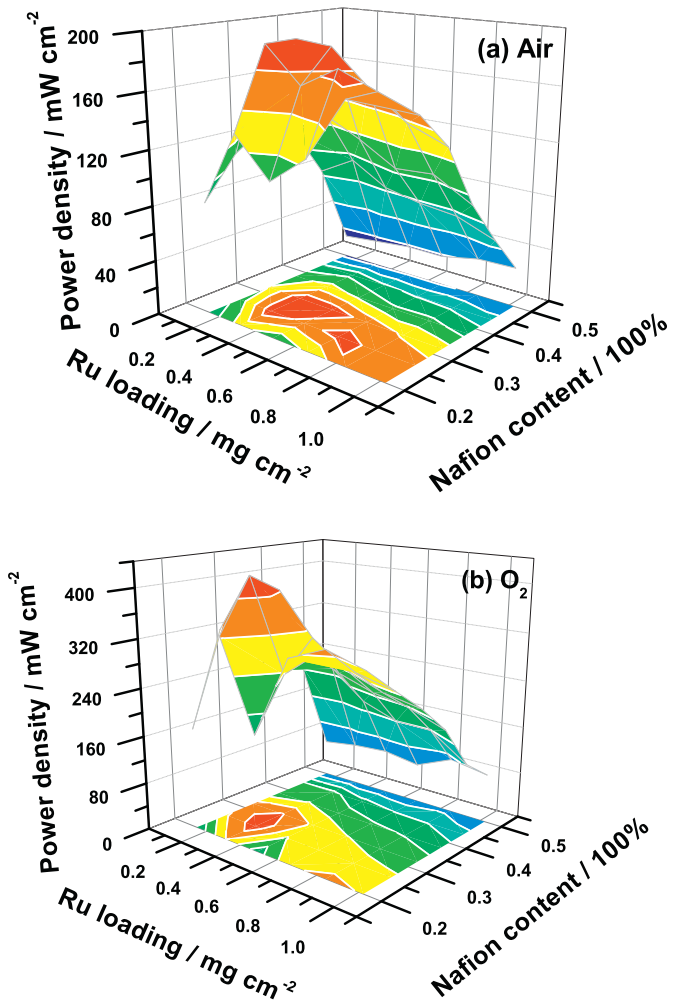

Fig. 8. Effects of Ru loads and Nafion content on peak power density obtained in the single cell tests at 65 °C under ambient pressure with (a) H_2/air: 100/250 ml min^{-1} and (b) H_2/O_2: 250/250 ml min^{-1}. Anode: 40% Pt/C, 0.256 mg Pt cm^{-2}, cathode: $Ru_{85}Se_{15}$/CA-XC72R, Nafion-212.

per unit mass Ru) of 700 and 1470 mW mg^{-1}, in the H_2/air and H_2/O_2 fuel cells, respectively. However, the best catalyst utilization was achieved at 0.14 mg Ru cm^{-1}, which led to P_{max}^{mass} as high as 917 and 2460 mW mg^{-1}, approximately doubled that at 0.27 mg Ru cm^{-2} in the H_2/O_2 fuel cells. Table 1 summarizes the fuel cell performances of Ru_xSe_y catalysts under different operating conditions reported from available literatures. It is evident from Table 1 that the $Ru_{85}Se_{15}$ catalysts prepared at the current optimal 33% Nafion contents exhibited excellent cell performances and catalyst utilizations at ambient pressure and 65 °C.

As discussed previously, the active catalyst sites and thickness of cathode catalyst layers depended strongly upon the Ru loads and Nafion contents, accordingly, significantly influenced the cell performances. In order to view simultaneous effects of Ru load and Nafion content on fuel cell performance, the relations among Nafion content, Ru load and P_{max} are presented as the three dimensional plots in Fig. 8. The optimal Nafion contents and Ru loads can be determined from the best performance zones indicated in red. The optimized Nafion content was near 33% when the $Ru_{85}Se_{15}$ catalyst loads were less than 0.8 and 0.6 mg Ru cm^{-2} in the H_2/air and H_2/O_2 fuel cells, respectively, while near 20% when the catalyst loads more than 0.8 and 0.6 mg Ru cm^{-2} in H_2/air and H_2/O_2 fuel cells, respectively. The best performance zones in oxygen (Fig. 8(b)) were much narrower than those in air (Fig. 8(a)) because of the

Table 1
Fuel cell performances of Ru_xSe_y at various Ru loads under different cell conditions.

Cathode catalyst/mg Ru cm^{-2}		Single cell operating condition			Membrane	Anode load/mg Pt cm^{-2}	MEA fabrication	Max. power density		Ref.
		Gas(A/C)/ml min^{-1}	Pressure/psi	T_{cell}/°C				mW cm^{-2}	mW mg^{-1}	
Ru_xSe_y/C	0.4	H_2/O_2 (400/400)	30/34	80	117	0.6	CCM	112	280	[23]
Ru_xSe_y/C	0.4[a]	H_2/O_2 (550/550)	14/14	80	115	0.4	Unspecified	75	–	[24]
$Ru_{85}Se_{15}$/C	0.4	H_2/O_2 (50/100)	29/29	80	212	0.3	GDM	400	1000	[25]
Se/Ru(Se)/C	0.15	H_2/air (300/500)	30/30	80	1135 × 2	0.25	Decal-CCM	128	853	[26]
Ru_xSe_y/C	0.5	H_2/O_2 (unspecified)	58/58	80	Unspecified	0.5	GDM	150	300	[27]
Ru/Se/C	0.22	H_2/O_2 (200/450)	Ambient	75	3 M inomer	2	GDM	150	682	[28]
$Ru_{85}Se_{15}/TiO_2$/C	0.5	H_2/O_2 (50/100)	29/29	80	212	0.4	GDM	310	620	[29]
Ru_xSe_y/C	0.4[a]	H_2/O_2 (400/400)	30/34	80	112	0.6	CCM	135	–	[13]
$Ru_{85}Se_{15}$/MWCNTs	0.14	H_2/air (100/250)	Ambient	65	212	0.256	CCM (ultrasonic)	166	1203	[15]
		H_2/O_2 (250/250)						380	2753	[15]
	0.14	H_2/air (100/250)						127	917	
$Ru_{85}Se_{15}$/C		H_2/O_2 (250/250)	Ambient	65	212	0.256	CCM (ultrasonic)	339	2456	Present work
	0.27	H_2/air (100/250)						190	704	
		H_2/O_2 (250/250)						400	1481	

[a] Ru_xSe_y loading.

enhanced catalyst utilization. At higher Ru loads the more active catalyst sites would be available, but the oxygen diffusion would become more predominated, while the mass transport limitations would become more severe due to the reduction in the gas pores by retarding the gas access to active sites with larger Nafion contents. Therefore, when using high Ru loads, low Nafion contents would be more beneficial to achieve good cell performance.

4. Conclusions

The electrodes with the $Ru_{85}Se_{15}$/CA-XC72R were prepared using catalyst coated membrane method with ultrasonic-spray technique. The dependences of cell performance on the Nafion content and Ru load were interpreted by the presence of active catalyst sites and the thickness of catalyst layers varied by the interfacial characteristics through the impedance analysis and SEM examination. The active sites might become the main rate-determining step at lower catalyst loads (<0.27 mg Ru cm^{-2}), while the catalyst layer might become thicker and oxygen diffusion becomes the main rate-determining step at higher catalyst loads (>0.27 mg Ru cm^{-2}) and higher Nafion contents (>33%). The optimal Nafion content was approximately 33% when the Ru loads were lower than 0.8 and 0.6 mg Ru cm^{-2} in the H_2/air and H_2/O_2 fuel cells, respectively. The excessive Nafion content resulted in blocks of oxygen diffusion, catalyst sites and water flooding, while the less Nafion content resulted in the decreases of three-phase interface and catalyst utilization. The optimal Nafion content was near 20% when the Ru loads was higher than 0.8 and 0.6 mg Ru cm^{-2} in the H_2/air and H_2/O_2 fuel cells, respectively. The addition of Nafion content to thick catalyst layers would cause serious mass transport limitations by retarding the gas access to active sites. The maximum peak power densities obtained with 0.27 mg Ru cm^{-2} and 33% Nafion at 65 °C under ambient pressure were 190 mW cm^{-2} at 620 mA cm^{-2} and 400 mW cm^{-2} at 1430 mA cm^{-2} in the H_2/air and H_2/O_2 fuel cells, respectively. However, the best catalyst utilizations, in terms of the maximum peak power density per unit mass Ru of 917 and 2460 mW mg^{-1}, were achieved in the H_2/air and H_2/O_2 fuel cells, respectively, with 0.14 mg Ru cm^{-2} and 33% Nafion.

Acknowledgments

The authors wish to thank the financial support from the Fujian Key Laboratory of Advanced Materials, China (2006L2003). Mr. Zheng also greatly appreciates the graduate student scholarship provided by Xiamen University and Yuan Ze University under the student exchange program.

References

[1] Y. Feng, A. Gago, L. Timperman, N. Alonso-Vante, Electrochim. Acta 56 (2011) 1009–1022.
[2] K.-H. Kim, K.-Y. Lee, H.-J. Kim, E. Cho, S.-Y. Lee, T.-H. Lim, S.P. Yoon, I.C. Hwang, J.H. Jang, Int. J. Hydrogen Energy 35 (2010) 2119–2126.
[3] B. Millington, V. Whipple, B.G. Pollet, J. Power Sources 196 (2011) 8500–8508.
[4] M. Prasanna, E.A. Cho, T.H. Lim, I.H. Oh, Electrochim. Acta 53 (2008) 5434–5441.
[5] Y. Song, J.M. Fenton, H.R. Kunz, L.J. Bonville, M.V. Williams, J. Electrochem. Soc. 152 (2005) A539–A544.
[6] G. Sasikumar, J.W. Ihm, H. Ryu, J. Power Sources 132 (2004) 11–17.
[7] D. Lee, S. Hwang, Int. J. Hydrogen Energy 33 (2008) 2790–2794.
[8] D. Song, Q. Wang, Z. Liu, M. Eikerling, Z. Xie, T. Navessin, S. Holdcroft, Electrochim. Acta 50 (2005) 3347–3358.
[9] A.J.J. Kadjo, P. Brault, A. Caillard, C. Coutanceau, J.P. Garnier, S. Martemianov, J. Power Sources 172 (2007) 613–622.
[10] E. Passalacqua, F. Lufrano, G. Squadrito, A. Patti, L. Giorgi, Electrochim. Acta 46 (2001) 799–805.
[11] H.A. Gasteiger, J.E. Panels, S.G. Yan, J. Power Sources 127 (2004) 162–171.
[12] C.-M. Lai, J.-C. Lin, F.-P. Ting, S.-D. Chyou, K.-L. Hsueh, Int. J. Hydrogen Energy 33 (2008) 4132–4137.
[13] R.G. González-Huerta, A. Guzman-Guzman, O. Solorza-Feria, Int. J. Hydrogen Energy 35 (2010) 12115–12119.
[14] K. Wippermann, B. Richter, K. Klafki, J. Mergel, G. Zehl, I. Dorbandt, P. Bogdanoff, S. Fiechter, S. Kaytakoglu, J. Appl. Electrochem. 37 (2007) 1399–1411.
[15] Q. Zheng, X. Cheng, T.-C. Jao, F.-B. Weng, A. Su, Y.-C. Chiang, Int. J. Hydrogen Energy 36 (2011) 14599–14607.
[16] Z. Xie, S. Holdcroft, J. Electroanal. Chem. 568 (2004) 247–260.
[17] M. Ciureanu, R. Roberge, J. Phys. Chem. B 105 (2001) 3531–3539.
[18] E. Barsoukov, J.R. Macdonald, Impedance Spectroscopy: Theory, Experiment, and Applications, second ed., Wiley-Interscience, New Jersey, 2005.
[19] X. Yuan, H. Wang, J. Colin Sun, J. Zhang, Int. J. Hydrogen Energy 32 (2007) 4365–4380.
[20] F. Liu, B. Yi, D. Xing, J. Yu, Z. Hou, Y. Fu, J. Power Sources 124 (2003) 81–89.
[21] N. Wagner, T. Kaz, K.A. Friedrich, Electrochim. Acta 53 (2008) 7475–7482.
[22] I.A. Schneider, D. Kramer, A. Wokaun, G.G. Scherer, J. Electrochem. Soc. 154 (2007) B770–B782.
[23] R.G. González-Huerta, J.A. Chávez-Carvayar, O. Solorza-Feria, J. Power Sources 153 (2006) 11–17.
[24] A. Kolary-Zurowska, A. Zieleniak, K. Miecznikowski, B. Baranowska, A. Lewera, S. Fiechter, P. Bogdanoff, I. Dorbandt, R. Marassi, P.J. Kulesza, J. Solid State Electrochem. 11 (2007) 915–921.
[25] G. Liu, H. Zhang, J. Hu, Electrochem. Commun. 9 (2007) 2643–2648.
[26] C. Delacote, A. Bonakdarpour, C.M. Johnston, P. Zelenay, A. Wieckowski, Faraday Discuss. 140 (2008) 269–281.
[27] M.J.F. Guinel, A. Bonakdarpour, B. Wang, P.K. Babu, F. Ernst, N. Ramaswamy, S. Mukerjee, A. Wieckowski, ChemSusChem 2 (2009) 658–664.
[28] A. Garsuch, X. Michaud, K. Böhme, G. Wagner, J.R. Dahn, J. Power Sources 189 (2009) 1008–1011.
[29] T. Xu, H. Zhang, H. Zhong, Y. Ma, H. Jin, Y. Zhang, J. Power Sources 195 (2010) 8075–8079.